Introducing Time-of-Flight and Resolution Recovery Image Reconstruction to Clinical Whole-body PET Parametric Imaging

Nicolas A. Karakatsanis[1,2], *Member, IEEE*, Martin A. Lodge[2], Arman Rahmim[2,5], *Senior Member, IEEE*, and Habib Zaidi[1,3,4], *Senior Member, IEEE*

Abstract – **We recently proposed a dynamic multi-bed acquisition scheme enabling whole-body FDG PET parametric imaging from limited axial field-of-view PET/CT scanners in clinically feasible scan times. However, the proposed framework was only evaluated for standard ordered subsets expectation maximization (OSEM) reconstruction. Currently, state-of-the-art commercial PET/CT scanners are equipped with advanced detection systems, capable of measuring the time-of-flight (TOF) of each annihilated photon enabling to confine the location of the annihilation position to a small segment within the line of response. As such, noise propagation is reduced and TOF reconstruction may provide superior contrast to noise ratio (CNR). Furthermore, image reconstruction is enriched with the feature of scanner resolution point spread function (PSF) modeling within the system response matrix of OSEM algorithm, similarly allowing for higher CNR. In this study, we extended TOF and PSF modeling to the dynamic multi-bed domain and systematically investigated their impact on the quality of wholebody PET parametric images. The state-of-the-art Siemens Biograph mCT scanner and its reconstruction suite were utilized. An extensive set of realistic 4D phantom simulations for the mCT scanner with and without TOF features were performed. Resolution degradation was applied to match a spatial resolution of 4.5mm. Then, TOF and non-TOF reconstructed images with and without resolution modeling were produced. Subsequently, the impact of TOF and PSF was assessed for standard and generalized Patlak models. Our results demonstrate the potential benefit of introducing TOF and PSF in parametric imaging, with both features providing superior noise vs. bias trade-off. Tumor-to-background ratio is enhanced by 30% when utilizing TOF, while CNR is improved by 40% and 60% when either TOF or PSF capabilities are introduced, respectively. Finally, total CNR enhancement approaches 100% if the two features are combined.**

I. INTRODUCTION

WHOLE-BODY dynamic PET/CT acquisitions efficiently combine the benefits of multi-bed acquisitions for a large axial field-of-view (FOV) covering the whole-body (WB) [1] with those of dynamic acquisitions for 4D PET scans across time [2-11]. Recently, we presented such an imaging framework for PET tracers labeled with [18]F (e.g. FDG or FLT) enabling generation of whole-body parametric images from PET/CT scanners of limited axial FOV in clinically feasible scan times [12,13]. However, the framework was optimized and evaluated on regular OS-EM reconstructions without exploiting the potential of recent technological developments in PET acquisition and system matrix response modeling [14].

Currently, modern PET/CT scanners are equipped with fast counting systems capable of recording, with reasonable accuracy, known as time resolution, the time point at which each of the two annihilated photons of each coincidence event are detected (arrival times). These data can then be exploited to calculate the time required for each photon to travel from the annihilation to detection point, known as time-of-flight (TOF) [15]. Thus, it is now possible to estimate not only the line of response (LOR) connecting the two detectors of each coincidence event, but also the actual position of the annihilation event along the LOR, with a certain uncertainty, which is determined by the time resolution of the PET counting system. Thus, TOF acquisition capability can provide superior spatial resolution for matched noise levels in PET images. Furthermore, state-of-the-art reconstruction software of modern PET scanners has recently been supported with advanced system response matrices capable of exploiting highly detailed 3D finite resolution response measurements across the FOV of corresponding PET systems in order to more accurately model their resolution response. These methods, known as resolution modeling approaches, can enhance contrast and reduce spatial noise in the image domain at the cost of slower convergence rate [16].

Our aim, in this study, is to utilize TOF and resolution modeling reconstruction technologies in dynamic multi-bed acquisition and reconstruction methods in order to systematically investigate their impact on the quality of the final whole body PET parametric images as estimated indirectly from the reconstructed frames. For that purpose, we employ the state-of-the-art Siemens Biograph mCT TOF human PET scanner and its computationally efficient reconstruction tools [17]. The assessment is performed on two types of whole-body parametric images, each estimated by different Patlak-based FDG kinetic models, and was based both on realistic simulated as well as real clinical whole-body dynamic PET data.

II. METHODS AND MATERIALS

A. Clinical multi-bed dynamic acquisition protocol

We designed a clinically adoptable whole-body 4D acquisition protocol allowing for the production of both simulated and clinical dynamic projection data that can, subsequently, be reconstructed with or without TOF or resolution modeling features. Later, the resulting sets of dynamic whole-body passes can be analyzed by Patlak graphical analysis methods to produce respective whole-body parametric images for each case (Fig. 1).
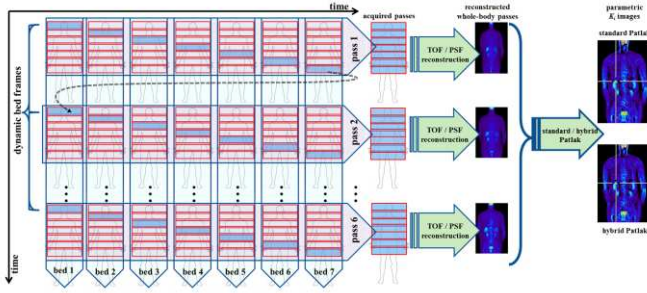
Fig. 1 Flow-chart of the second phase of multi-bed dynamic acquisition, the utilization of TOF and PSF reconstruction and the subsequent parametric imaging

We have proposed an optimal multi-bed dynamic PET acquisition protocol, involving an initial 6-min dynamic cardiac scan (1st phase), followed by a series of unidirectional multi-bed passes (2nd phase), covering the whole-body FOV and consisting of equal dynamic bed frames, each of 45sec [13]. Currently, we are also proposing an optimal acquisition time-window position, w.r.t. injection time, for the second phase of the protocol, consisting of a fixed number of 6 whole-body passes of total duration of ~35min [18].

B. Time-of-flight (TOF)-based reconstruction

Recent technological advances in detector time response systems have allowed state-of-the-art PET/CT systems, such as the Siemens Biograph mCT, to acquire TOF information for each coincidence event [15,17]. In non-TOF acquisitions, the coincidence counts at each detector pair bin are uniformly distributed across the whole LOR during the back-projection operation, regardless of the actual position of the annihilation within that LOR. On contrary, TOF data, if available, can be utilized to estimate within a certain uncertainty, a segment of the LOR where the annihilation point of each coincidence count is more probable to be located. As a result, in TOF-supported back-projection operations, counts at each detector bin can be more accurately distributed across different segments of the same LOR, reducing the propagation of noise during reconstruction (Fig. 2) [15]. The accuracy of the estimated counts distribution over each LOR is limited by the intrinsic time resolution of the scanner (527.5psec for the mCT) [17]. The smaller the differences in photon time-of-flights a scanner can discriminate, the higher the number of

LOR segments across which the LOR counts can be distributed during back-projection. Therefore, the better the time resolution of a TOF PET system, the more accurate can be the localization of the projection counts in the image space. Subsequently, TOF reconstruction exploits this added benefit of TOF information to achieve better spatial resolution at matched noise levels, compared to non-TOF, and superior contrast recovery [15]. On the other hand, TOF capability is also associated with larger sizes of projection data and considerably higher computational cost for the reconstruction process, since the data complexity increases linearly with the number of LOR segments, known as TOF bins [15]. In this work, we focus on investigating the impact of TOF in the dynamic whole-body passes and the resulting parametric images, particularly at regions with high noise, such as tumors of low uptake.
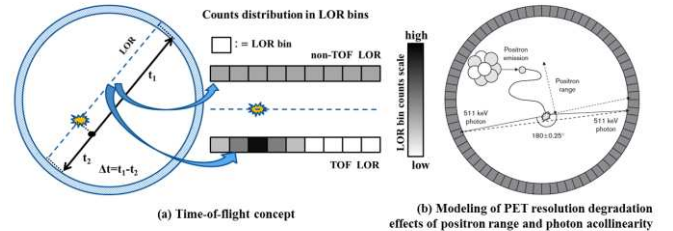
Fig. 2 (a) Utilization of TOF for each annihilated photon allows for more accurate distribution of counts in the LOR bins

C. Resolution modeling in image reconstruction
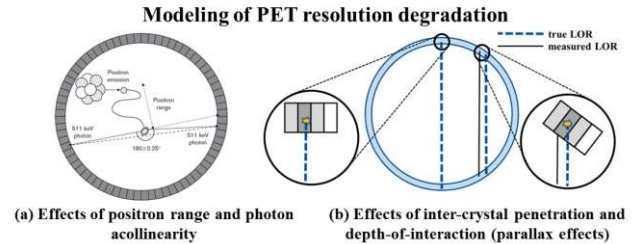
Fig. 3 PET resolution degradation effects due to a) positron range and photon acollinearity and b) inter-crystal penetration and depth of interaction uncertainty

In addition, advanced resolution recovery reconstruction algorithms have been recently introduced on commercial PET/CT scanners [16,17]. Detailed evaluation of the finite resolution or point spread function (PSF) response of a PET scanner across its entire FOV can be exploited later by the OS-EM reconstruction algorithm to more accurately model the overall resolution response within the iterative estimation process [16]. PET resolution degradation can be the result of the combined effect of both physical factors, such as positron range and photon acollinearity (Fig. 3a), as well as PET detector ring design limitations, such as inter-crystal penetration and crystal depth of interaction uncertainty (Fig. 3b).

By incorporating the overall PSF resolution kernel to the system matrix of the OS-EM reconstruction, we can achieve

better contrast recovery at matched noise levels [16]. Our purpose here is to apply PSF reconstruction to all dynamic passes to evaluate the impact of the above enhancements to the parametric image domain as well (Fig. 1).

D. Kinetic analysis and estimation of whole-body parametric images

In Figure 4(a) the standard 2-compartment 4-parameter kinetic model for FDG tracer is presented.
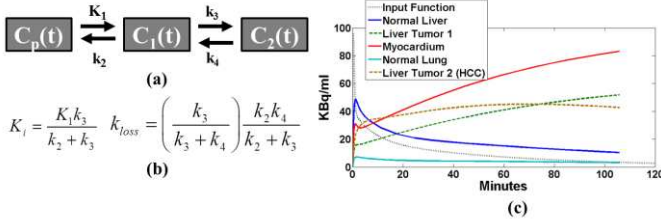
Fig. 4 (a) The kinetic model for FDG tracer, where $C_p(t)$, $C_1(t)$ and $C_2(t)$ are the input function, the non-metabolized and the metabolized tracer concentration in tissue, respectively, (b) the definitions of macro-parameters K_i and k_{loss} and (c) the modeled TACs for different regions, as generated by the model in (a).

Assuming irreversibility of compartment $C_2(t)$, i.e. $k_4=0$, the standard Patlak method simplifies this model (Eq. 1) by introducing the macro-parameter of the tracer influx rate constant K_i (Fig. 4b) [19]:

$$\frac{C(t)}{C_p(t)} = K_i \frac{\int_0^t C_p(\tau)d\tau}{C_p(t)} + V, t > t^* \qquad (1)$$

Eq. (1) is valid only for $t > t^*$, where t^* is the time after which relative kinetic equilibrium is attained between the plasma tracer concentration $C_p(t)$ (input function) and the tissue free (non-metabolized) tracer concentration $C_1(t)$ [19]. Ordinary least squares (OLS) regression can be applied to estimate Patlak parameters of K_i and V from the linear Eq. (1).

However, studies have reported reversibility of FDG compartment $C_2(t)$ for tumors [2,20,21]. In such cases, we have demonstrated erroneous estimation of K_i with the standard Patlak method [22]. Thus, we propose a generalized Patlak method (Eq. 2) accounting for such irreversibility by introducing the extra macro-parameter of tracer efflux rate constant k_{loss} (Fig. 4b) [19,22]:

$$\frac{C(t)}{C_p(t)} = K_i \frac{\int_0^t e^{-k_{loss}(t-\tau)}C_p(\tau)d\tau}{C_p(t)} + V, t > t^* \qquad (2)$$

The Basis Function Method (BFM) can be employed to estimate the generalized Patlak parameters (K_i, k_{loss}, V) from Eq. (2) [23]. The resulting estimates may, however, become very noisy at low count levels. Therefore, we have suggested:

i) initially calculating the correlation with Patlak method for all voxel TACs, followed by

ii) selective application the generalized Patlak method with BFM estimation only to the highly correlated voxel TACs and

the simplified Patlak method with OLS estimation to the rest (hybrid Patlak method) [22].

E. Realistic 4D simulations of FDG tracer kinetics

We conducted an extensive series of realistic 4D simulations of the Siemens Biograph mCT PET/CT scanner. The simulated FDG TACs are generated from a validated set of kinetic parameters obtained from the literature (Table I) and assigned to the corresponding regions of the XCAT phantom to produce noise-free dynamic images [24-26].

TABLE I. KINETIC RATE CONSTANTS PARAMETERS

Regions	K_1	k_2	k_3	k_4	V_B
Normal Liver	0.864	0.981	0.005	0.016	-
Liver Tumor	0.243	0.78	0.1	0	-
Normal Lung	0.108	0.735	0.016	0.013	0.017
Liver Tumor 2	0.283	0.371	0.057	0.012	-
Myocardium	0.6	1.2	0.1	0.001	-

Subsequently, the noise-free frames were forward projected, adding normalization, attenuation and scatter effects to simulate either non-TOF or TOF realistic projections with PSF resolution degradation matching a spatial resolution of 4.5mm FWHM. Then, randoms and quantitative levels of noise were added and the resulting projections were reconstructed with or without TOF and PSF modeling accordingly (6 iterations, 14 subsets) using e7tools [16]. The PSF kernel modeled in the PSF reconstructions was derived by reducing its FWHM width in axial direction by 10% compared to simulations, in an attempt to limit Gibbs ringing artifacts, a commonly observed effect in resolution recovery reconstruction algorithms [16],[27-29]. A systematic investigation of the PSF kernel width effect has demonstrated a potential enhancement in reproducibility and bias as well as a reduction in ringing Gibbs artifacts when the FWHM width of the kernel is slightly underestimated in PSF reconstructions with respect to the true underlying PSF response [30,31].

III. RESULTS AND DISCUSSION

In Fig. 5, we present simulation results for the 1st and 6th reconstructed dynamic frames for three different numbers of iterations as well as the respective standard and hybrid Patlak K_i parametric images for all combinations of TOF and PSF features with and without noise.

Furthermore, Fig. 6(a) presents a comparative evaluation of the noise vs. bias trade-off exhibited in the Patlak K_i images, when indirectly estimated from OSEM dynamic PET simulated frames, the latter reconstructed from different iterations each time either with or without TOF or PSF features. A liver tumor (labeled "liver tumor 2" in Table I) region of interest (ROI) was selected for the evaluation of noise and bias across the different image data sets. A similar noise-bias trade-off performance trend was also observed for the case of the indirectly estimated hybrid Patlak K_i images from the same set of simulated PET frames. Moreover, the clinically relevant figures of merit of tumor-to-background ratio (TBR contrast) and contrast-to-noise ratio (CNR) were

evaluated on the same K_i images for the same number of iterations.
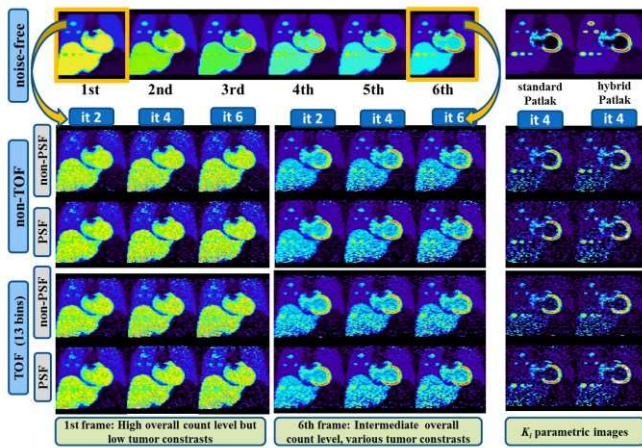
Fig. 5 Comparative evaluation of noise-free and noisy simulated dynamic frames and K_i parametric images for all combinations of TOF and PSF reconstruction schemes and the two Patlak estimation methods.
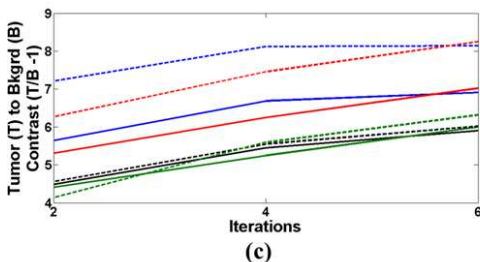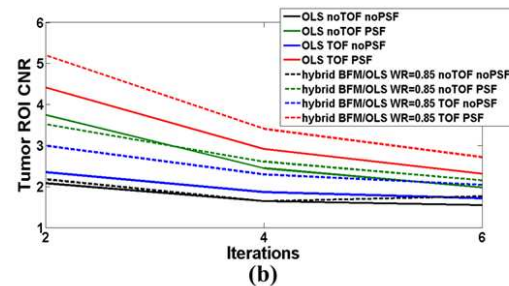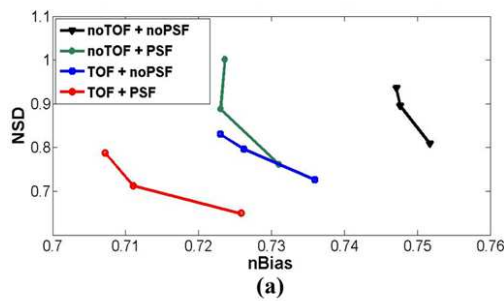
Fig. 6 (a) Noise vs. bias plot (b) TBR and (c) CNR performance evaluation for a liver tumor region (with kinetics presented in Table I) for the standard and hybrid Patlak K_i parametric images, when reconstructed with or without TOF and PSF features

The simulated results in Fig. 5 and particularly the quantitative analysis in Fig. 6 illustrate the superior K_i image quality when either TOF or PSF features are enabled with the best results produced when the two features are combined. In terms of noise-bias trade-off performance (fig. 6a), the addition of PSF modeling alone improved resolution/bias, while the addition of TOF alone produced superior resolution and lower noise resulting in better resolution, compared to PSF alone, at matched noise levels. A similar noise-bias trade-off performance enhancement was also observed for the case of hybrid Patlak images.

Moreover, as the results in fig. 6(b) and 6(c) suggest, both TBR contrast and CNR in the selected liver tumor regions were improved with the added features of TOF and PSF reconstruction. While tumor CNR in the case of combined TOF and PSF utilization is superior in our simulations for all iterations, the TBR contrast for the same case only outperforms the case of TOF without PSF at later iterations. This behavior can be attributed to the slower convergence of the PSF reconstruction resulting in lower contrast at earlier iterations for TOF+PSF compared to TOF alone.

Finally, in all cases, hybrid Patlak achieved consistently higher TBR and CNR metrics than standard Patlak, which can be attributed to the presence of reversible FDG uptake (i.e. $k_4>0$), which generalized Patlak model takes into account while standard Patlak assumes it to be zero [19,22].
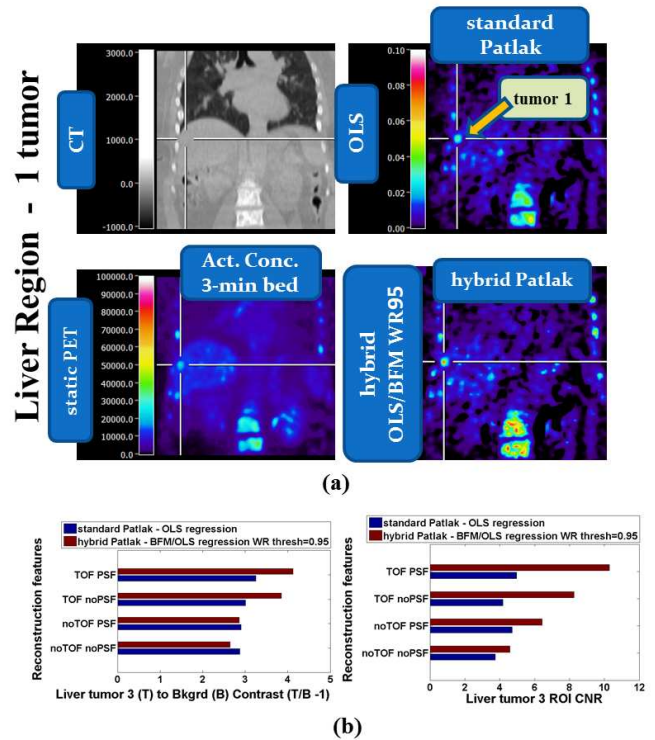
Fig. 7 (a) Comparative evaluation of Patlak (standard and hybrid) vs. static PET images (3min acquisition per bed) in the liver region of clinical dynamic whole-body PET data, corresponding CT is provided for reference. In all PET images, TOF and PSF features are activated. (b) TBR (bottom left) and CNR (bottom right) performance evaluation in the region of the identified liver tumor for the respective standard and hybrid K_i clinical images reconstructed with or without TOF and PSF features.

In Figs 7 and 8, the effect of TOF acquisition and PSF reconstruction on clinical WB dynamic PET data is demonstrated. Figs 7(a) and 8(a) presents the static PET vs. the parametric K_i whole-body patient images, when both TOF and PSF features are activated, for a tumor case in the liver and two cases in the thorax region respectively. Then, Fig. 7(b) demonstrates the quantitative effect of TOF and PSF technologies on the tumor to background (TBR) and contrast-to-noise (CNR) ratios, as they were evaluated over an ROI drawn in the patient liver region, labeled as "tumor 1". The quantitative TBR and CNR performance analysis is repeated in fig. 8(b) and (c) for another two suspected tumor cases, this time in the thorax region of another patient, labeled as "tumor 1" and "tumor 2" respectively.

(a)

(b)

(c)
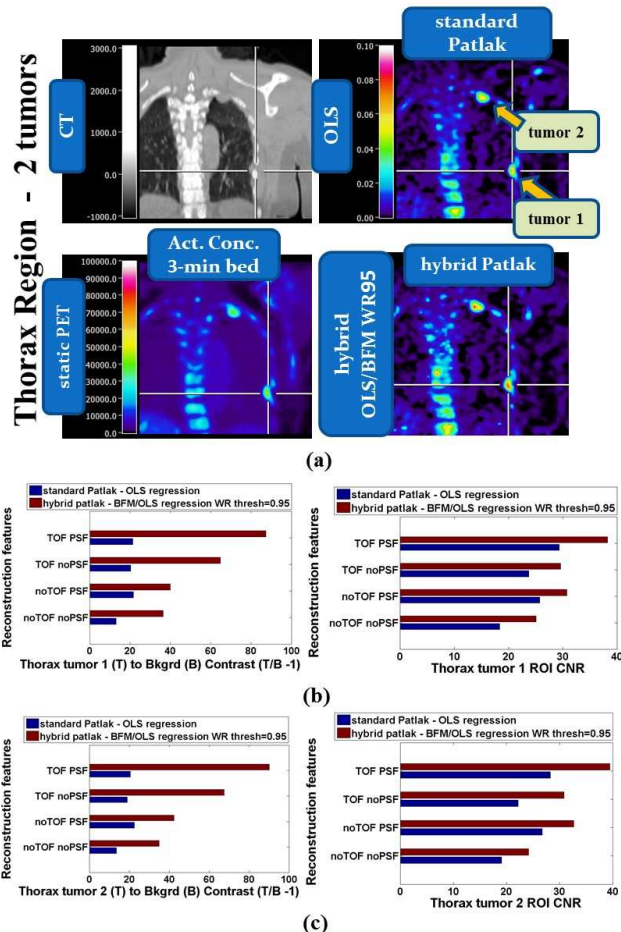
Fig. 8 (a) Comparative evaluation of Patlak (standard and hybrid) vs. static PET images (3min acquisition per bed) in the region of the thorax from clinical dynamic whole-body PET data, corresponding CT is provided for reference. In all PET images, TOF and PSF features are enabled. (b) and (c) TBR (left) and CNR (right) performance evaluation in the thorax region for two identified suspected tumor regions for the respective standard and hybrid K_i clinical images reconstructed with or without TOF and PSF features.

The quantitative evaluation on clinical studies confirms our findings from the analysis of the simulation study. In all examined patient cases, a total of three suspected tumor regions across multiple clinical WB dynamic PET/CT scans were identified, where the introduction of TOF or PSF features alone, enhanced both TBR and CNR metrics on parametric Patlak K_i images, with the best performance

observed when the two features were combined. In addition, the hybrid Patlak images were in all cases exhibiting higher TBR and CNR evaluations in comparison to the standard Patlak images.

Finally, the advent of TOF and PSF although already taking advantage of both standard and hybrid Patlak image generation methods, had a stronger effect for the hybrid Patlak images, particularly in the case of TBR performance. This is attributed to our findings that generalized and, thus, hybrid Patlak imaging involves a non-linear parametric estimation method and thus is more susceptible to the high levels of noise usually present in whole-body dynamic PET data [22]. Therefore, when combining TOF acquisition with PSF reconstruction, the noise propagation can be limited during reconstruction, an effect particularly welcomed by hybrid Patlak and, in general, non-linear parametric image estimation processes.

IV. CONCLUSIONS AND FUTURE PROSPECTS

In this study, the quantitative benefits of introducing TOF acquisition and PSF modeling in the process of whole-body PET parametric imaging have been demonstrated both in simulations and clinical studies. The noise-bias trade-off performance analysis on the simulated data quantified the degree of noise reduction and resolution enhancement for matched noise levels when either TOF or PSF technologies are utilized alone, with the best outcome observed when combined.

Whole-body parametric PET imaging, even without TOF and PSF utilization, has already been shown to deliver images of enhanced tumor contrast and better reproducibility mainly because it relies on more quantitative surrogate metrics such as tracer uptake rate K_i vs. the standardized but semi-quantitative SUV metric derived from static PET studies. However, it also suffers from higher levels of noise and considerable time gaps in acquisition of the complete kinetic range of PET tracers such as FDG, limiting the choice of appropriate kinetic models applicable to this type of studies. In this study we demonstrated how TOF acquisitions and PSF modeling can further enhance the statistical quality of the dynamic projection data and the modeling process within the reconstruction to assist Patlak models in more accurately and precisely estimating whole-body parametric images from dynamic PET studies. Our findings here encourages us to believe that the advent of these two types of technologies, which both are already present in current clinical PET scanners, together with the application of the standard or our proposed generalized Patlak models, can facilitate the faster transition of this quantitative PET imaging framework to the clinic in the near future.

In addition, the results of this study imply a positive effect of TOF and PSF modeling also for conventional single-bed dynamic PET imaging either in the case of the less challenging graphical analysis methods or, particularly, for the more demanding and highly susceptible to noise fully compartmental kinetic modeling processes.

Currently, we are also investigating the relative effect of these two types of technology in the context of direct 4D

whole-body parametric image reconstruction using either the standard or the generalized Patlak model [32,33].

V. ACKNOWLEDGMENTS

REFERENCES

[1] R. L. Wahl and J. W. Buchanan, "Principles and Practice of Positron Emission Tomography" Book Chapter (Philadelphia, PA: Lippincott Williams & Wilkins), 2002

[2] C. Messa, Y. Choi, C.K. Hoh, E.L. Jacobs, J.A. Glaspy, S. Rege, E. Nitzsche, S. C. Huang, M. E. Phelps, and R. A. Hawkins, "Quantification of glucose utilization in liver metastases: parametric imaging of FDG uptake with PET," J. Comp. Assist. Tomography, vol. 16, no. 5, p. 684, 1992

[3] K. R. Zasadny and R. L. Wahl "Enhanced FDG-PET tumor imaging with correlation-coefficient filtered influx-constant images," J. Nucl. Med., 37(2), p. 371-374, 1996

[4] I. C. Smith, A. E. Welch, A. W. Hutcheon, I. D. Miller, S. Payne, F. Chilcott, S. Waikar, T. Whitaker, A. K. Ah-See, O. Eremin, S. D. Heys, F. J. Gilbert and P. F. Sharp, "Positron emission tomography using [18F]-fluorodeoxy-D-glucose to predict the pathologic response of breast cancer to primary chemotherapy," J. Clin. Onc., 18(8), 1676-1688, 2000

[5] D. Thorwarth, S. M. Eschmann, F. Paulsen and M. Alber, "A kinetic model for dynamic [18F]-Fmiso PET data to analyse tumour hypoxia," Phys. Med. Biol., 50(10), p. 2209, 2005

[6] T. Schroeder, M. F. V. Melo, G. Musch, R. S. Harris, T. Winkler, and J. G. Venegas "PET imaging of regional 18F-FDG uptake and lung function after cigarette smoke inhalation," J. Nucl. Med., 48(3), p. 413-419, 2007

[7] A. Dimitrakopoulou-Strauss, L. Pan, and L. G. Strauss, "Parametric imaging a promising approach for the evaluation of dynamic PET-18 F-FDG studies-the DKFZ experience," Hel. J. Nucl. Med., 13(1), p. 18-22, 2010

[8] W. Wang, N. Y. Lee, J. C. Georgi, M. Narayanan, J. Guillem, H. Schöder and J. L. Humm, "Pharmacokinetic analysis of hypoxia 18F-fluoromisonidazole dynamic PET in head and neck cancer," J. Nucl. Med., 51(1), p. 37-45, 2010

[9] D. J. Apostolopoulos, A. Dimitrakopoulou-Strauss, P. Hohenberger, S. Roumia and L. G. Strauss, "Parametric images via dynamic 18F-fluorodeoxyglucose positron emission tomographic data acquisition in predicting midterm outcome of liver metastases secondary to gastrointestinal stromal tumours," Eur J Nucl. Med. and Mol. Imaging, 38(7), p. 1212-1223, 2011

[10] N. A. Karakatsanis, M. A. Lodge, Y. Zhou, J. Mhlanga, M. Chaudhry, A. K. Tahari, R. L. Wahl and A. Rahmim, "Towards parametric whole-body FDG PET/CT imaging: potentials for enhanced tumor detectability" J Nucl Med. 2012; 53 (Supplement 1):1236, 2012

[11] G. Tomasi, F. Turkheimerand E. Aboagye, "Importance of quantification for the analysis of PET data in oncology: review of current methods and trends for the future," Molecular Imaging and Biology, 14(2), p. 131-146, 2012

[12] N. A. Karakatsanis, M. A. Lodge, A. K. Tahari, Y. Zhou, R. L. Wahl and A. Rahmim, "Dynamic whole-body PET parametric imaging: I. Concept, acquisition protocol optimization and clinical application," Phys. Med. Biol. 58(20), p. 7391, 2013

[13] N. A. Karakatsanis, M. A. Lodge, Y. Zhou, R. L. Wahl and A. Rahmim, "Dynamic whole-body PET parametric imaging: II. Task-oriented statistical estimation. Phys. Med. Biol. 58(20), p. 7419, 2013

[14] N. A. Karakatsanis, M. A. Lodge, Y. Zhou, J. Mhlanga, M. A. Chaudhry, A. K. Tahari, R. L. Wahl and A. Rahmim, "Dynamic multi-bed FDG PET imaging: feasibility and optimization," Nuclear Science Symposium and Medical Imaging Conference (NSS/MIC), Valencia, Spain, p. 3863-3870, 2011

[15] J. S. Karp, S. Surti, M. E. Daube-Witherspoon and G. Muehllehner, "Benefit of time-of-flight in PET: experimental and clinical results," J. Nucl. Med., 49(3), p. 462-470, 2008

[16] V. Y. Panin, F. Kehren, C. Michel and M. E. Casey "Fully 3-D PET reconstruction with system matrix derived from point source measurements," IEEE Trans. in Med. Imag., 25(7), p. 907-921, 2006

[17] B.W. Jakoby, Y. Bercier, M. Conti, M.E. Casey, B. Bendriem and D.W. Townsend "Physical and clinical performance of the mCT time-of-flight PET/CT scanner," Phys. Med. Biol., 56(8), p.2375, 2011

[18] N. A. Karakatsanis, M. A. Lodge, M. E. Casey, H. Zaidi and A. Rahmim, "Impact of Acquisition Time-Window on Clinical Whole-Body PET Parametric Imaging," Nuclear Science Symposium and Medical Imaging Conference (NSS/MIC), Seattle, WA, USA, 2014

[19] C.S. Patlak and R.G. Blasberg, "Graphical evaluation of blood-to-brain transfer constants from multiple-time uptake data. Generalizations," J. Cereb Blood Flow Metab, 5, p. 584, 1985.

[20] G. A. Sayre, B. L. Franc and Y. Seo "Patient-specific method of Generating Parametric Maps of Patlak K_i without Blood Sampling or Metabolite Correction: A Feasibility Study.", Int. J. Mol. Imag., 2011.

[21] C. K. Hoh, C. Vera and C. Schiepers, "Reducing effects of non-zero k_4 and metabolites in generating Patlak parametric images of FLT uptake," J Nucl Med; 52 (Supplement 1): 2063, 2011

[22] N. A. Karakatsanis, Y. Zhou, M. A. Lodge, M. E. Casey, R. L. Wahl and A. Rahmim, "Quantitative whole-body parametric PET imaging incorporating a generalized Patlak model," Nuclear Science Symposium and Medical Imaging Conference (NSS/MIC), Seoul, S. Korea, 2013

[23] R. N. Gunn, A.A. Lammertsma, S.P. Hume and V.J. Cunningham, "Parametric imaging of ligand-receptor binding in PET using a simplified reference region model," Neuroimage, 6(4), p. 279, 1997

[24] A. Dimitrakopoulou-Strauss, V. Georgoulias, M. Eisenhut, F. Herth, S. Koukouraki, H. Macke, U. Haberkorn, and L. Strauss, "Quantitative assessment of SSTR2 expression in patients with non-small cell lung cancer using 68 Ga-DOTATOC PET and comparison with 18 F-FDG PET," Eur J Nucl. Med. and Mol. Imaging, vol. 33, no. 7, p. 823–830, 2006.

[25] S. Okazumi, A. Dimitrakopoulou-Strauss, M. Schwarzbach, and L. Strauss, "Quantitative, dynamic 18F-FDG-PET for the evaluation of soft tissue sarcomas: relation to differential diagnosis, tumor grading and prediction of prognosis," Hel. J. Nucl. Med., vol. 12, no. 3, p. 223, 2009

[26] T. Torizuka, N. Tamaki, T. Inokuma, Y. Magata, S. Sasayama, Y. Yonekura, A. Tanaka, Y. Yamaoka, K. Yamamoto, J. Konishi et al., "In vivo assessment of glucose metabolism in hepatocellular carcinoma with FDG-PET," J. Nucl. Med., vol. 36, no. 10, p. 1811, 1995.

[27] A. Reader, P. J. Julyan, H. Williams, D. L. Hastings and J. Zweit, "EM algorithm system modeling by image-space techniques for PET reconstruction," IEEE Trans. Nucl. Sc., 50(5), 1392-1397, 2003

[28] A. Rahmim, J. Qi and V. Sossi, "Resolution modeling in PET imaging: Theory, practice, benefits, and pitfalls," Med. Phys., 40(6), 064301, 2013

[29] A. Rahmim and J. Tang, "Noise propagation in resolution modeled PET imaging and its impact on detectability," Phys. Med. Biol., 58(19), 6945, 2013

[30] S. Ashrafinia, N. A. Karakatsanis, H. Mohy-ud-Din, and A. Rahmim "Towards continualized task-based resolution modeling in PET imaging," Proc. SPIE 9033, Medical Imaging 2014: Physics of Medical Imaging, 903327, 2014

[31] S. Ashrafinia, H. Mohy-ud-Din, N. A. Karakatsanis, D. J. Kadrmas, and A. Rahmim, "Enhanced quantitative PET imaging utilizing adaptive partial resolution modeling," J. Nucl. Med., vol. 55 (suppl. 1): 371, 2014

[32] N. A. Karakatsanis, M. A. Lodge, R. L. Wahl and A. Rahmim, "Direct 4D whole-body PET/CT parametric image reconstruction: concept and comparison vs. indirect parametric imaging," J Nucl Med. 2013; 54 (Supplement 2):2133, 2013

[33] N. A. Karakatsanis and A. Rahmim, "Whole-body PET parametric imaging employing direct 4D nested reconstruction and a generalized non-linear Patlak model," Proc. SPIE 9033, Medical Imaging 2014: Physics of Medical Imaging, 90330Y, 2014